Northeast Asian dust storms: Real-time numerical prediction and validation

Yaping Shao,[1] Yan Yang,[1] Jianjie Wang,[2] Zhenxin Song,[2] Lance M. Leslie,[3] Chaohua Dong,[4] Zhihuang Zhang,[5] Zhaohui Lin,[6] Yutaka Kanai,[7] Sadayo Yabuki,[8] and Youngsin Chun[9]

Received 6 April 2003; revised 23 June 2003; accepted 29 July 2003; published 18 November 2003.

[1] This study is concerned with the quantitative prediction of dust storms in real time. An integrated wind erosion modeling system is used for 24-, 48-, and 72-hour forecasts of northeast Asian dust events for March and April 2002. The predictions are validated with synoptic records from the meteorological network and dust concentration measurements at 12 stations in China, Japan, and Korea. The predicted spatial patterns and temporal evolutions of dust events and the predicted near-surface dust concentrations are found to agree well with the observations. The validation confirms the capacity of the modeling system in quantitative forecasting of dust events in real time. On the basis of the predictions, dust activities in northeast Asia are examined using quantities such as dust emission, deposition, and load. During an individual dust episode, dust sources and intensities vary in space and time, but on average the Gobi Desert, the Hexi (Yellow River West) Corridor, the Chaidam Basin, the Tulufan Basin, and the fringes of the Talimu and Zhunge'er Basins are identified to be the main source regions. The Gobi Desert is the strongest dust source, where the maximum dust emission reaches 5000 $\mu g\ m^{-2}\ s^{-1}$ and the net dust emission reaches 16 t $km^{-2}\ d^{-1}$ in March and April 2002. Net dust deposition covers a large area, with the Loess Plateau receiving about 1.6 to 4.3 t $km^{-2}\ d^{-1}$. A zone of high dust load exists along the northern boundary of the Tibet Plateau, with a maximum of around 2 t km^{-2} situated over the Gobi Desert. The total dust emission, total dust deposition, and total dust load for the domain of the simulation are estimated. The average (maximum) total dust emission is 11.5×10^6 (65.7×10^6) t d^{-1}, the average (maximum) total dust deposition is 10.8×10^6 (51.4×10^6) t d^{-1}, and the average (maximum) total dust load is 5.5×10^6 (15.9×10^6) t. *INDEX TERMS:* 0305 Atmospheric Composition and Structure: Aerosols and particles (0345, 4801); 1610 Global Change: Atmosphere (0315, 0325); 1620 Global Change: Climate dynamics (3309); 3210 Mathematical Geophysics: Modeling; 3322 Meteorology and Atmospheric Dynamics: Land/atmosphere interactions; *KEYWORDS:* dust storm, aerosol, numerical prediction

Citation: Shao, Y., et al., Northeast Asian dust storms: Real-time numerical prediction and validation, *J. Geophys. Res.*, *108*(D22), 4691, doi:10.1029/2003JD003667, 2003.

1. Introduction

[2] We are concerned with the quantitative prediction of dust storms in real time, with a focus on northeast Asia. There are two motivations for this work: (1) The arid and semiarid regions of northeast Asia are major sources of mineral dust which plays an important role in the global aerosol cycle. Hence the prediction of dust concentration and size characteristics is an important issue in atmospheric research [e.g., *Sokolik et al.*, 1998]. (2) From spring to early summer, dust storms frequently occur in northeast Asia. Severe dust storms may result in the loss of human lives and the disruption of social and economic activities. The real-time prediction of dust storms therefore is highly desirable as a meteorological service to the public.

[3] In recent years, studies of northeast Asian dust storms have been made through large-scale field observations [*Mikami et al.*, 2002], numerical modeling [*Shao et al.*,

[1]Department of Physics and Materials Science, City University of Hong Kong, Hong Kong, China.
[2]National Meteorology Centre, China Meteorological Administration, Beijing, China.
[3]School of Meteorology, University of Oklahoma, Norman, Oklahoma, USA.
[4]National Satellite Meteorology Centre, China Meteorological Administration, Beijing, China.
[5]Institute of Geographical Sciences and Natural Resources Research, Chinese Academy of Sciences, Beijing, China.
[6]Institute of Atmospheric Physics, Chinese Academy of Sciences, Beijing, China.
[7]National Institute of Advanced Industrial Science and Technology, Tsukuba, Japan.
[8]Institute of Physical and Chemical Research, Saitama, Japan.
[9]Meteorological Research Institute, Korea Meteorological Administration, Seoul, Korea.

0148-0227/03/2003JD003667$09.00

2002; *Uno et al.*, 2001; *Wang et al.*, 2000], remote sensing [*Husar et al.*, 2001; *Prospero et al.*, 2002] and examining the climatic and land-surface conditions [*Dong et al.*, 2000; *Zhang et al.*, 2001]. In several studies published in the Chinese literature, dust storm frequencies in China have been examined using historical synoptic records [e.g., *Zhou*, 2001]. All these studies have resulted in a general understanding of the climatic and synoptic features of northeast Asian dust activities. However, reliable quantitative estimates of dust concentration, emission, transport and deposition are still not available.

[4] The prediction of dust activities, with quantitative confidence, is not possible unless the processes involved in the dust cycle, i.e., emission, transport and deposition are all adequately simulated. Many issues remain to be resolved in this field of research, but the most critical one is the quantification of dust sources. A survey of literature shows that in some previous studies, dust emissions were calculated with very simple schemes, some of which are too crude to be credible. More recently, better schemes for dust emission have been under development on the basis of wind erosion physics [*Marticorena and Bergametti*, 1995; *Shao et al.*, 1996; *Marticorena et al.*, 1997; *Lu and Shao*, 1999; *Alfaro and Gomes*, 2001; *Shao*, 2001].

[5] The prediction of dust activities requires the coupling of the dust emission scheme with an atmospheric model, supported by other modules and adequate land-surface parameter, i.e., the establishment of an integrated modeling system. Early examples of this approach are given by *Westphal et al.* [1988], *Joussaume* [1990], and *Gillette and Hanson* [1989]. *Shao and Leslie* [1997] and *Lu and Shao* [2001] developed an integrated wind erosion modeling system (IWEMS) which simulates all stages of dust cycle, from dust emission and transport to deposition. IWEMS is developed within the framework of a Computational Environmental Modeling System (CEMSYS4). A key component of CEMSYS4 is the high-resolution limited area atmospheric prediction model. IWEMS was implemented for modeling dust storms in Australia. *Shao et al.* [2002] further developed IWEMS by incorporating the new wind erosion scheme of *Shao* [2001] and applied the system to modeling two dust episodes in northeast Asia. *Wang et al.* [2000], *Nickovic et al.* [2001], *Uno et al.* [2001], and *Barnum et al.* [2003] reported the developments and applications of their dust prediction models.

[6] An outstanding issue with the study of *Shao et al.* [2002], as with other similar studies, is the unsatisfactory validation of the numerical results with high-quality measurements. This was largely due to the lack of such measurements at the time when the work was done. Despite the sophistication of the modeling system, the lack of validation undermines confidence in modeling results. Indeed, the uncertainties involved in the numerical simulation of dust events are believed to be large even with the best models currently available, as many aspects of the models, and dust emission in particular, are sensitive to input parameters such as soil type and vegetation cover.

[7] In 2002, we carried out continuous real-time forecasts of northeast Asian dust storms for March and April. In this paper, we first report a validation of the predicted spatial pattern and temporal evolution of northeast Asian dust events using synoptic records, and that of the predicted near-surface dust concentration using low-volume-sampler measurements at 12 stations in China, Japan and Korea. We then use the predictions to estimate the quantities for characterizing dust activities in northeast Asia, such as dust emission, dust deposition and dust load.

2. Integrated Modeling System and Land Surface Parameters

[8] IWEMS is composed of an atmospheric model, a land surface scheme, a wind erosion scheme, a transport and deposition scheme and a GIS (geographic information system) database. The atmospheric model is the host model which drives the other model components. The land surface scheme simulates the energy, momentum and mass exchanges between the atmosphere and the land surface but, most importantly for this study, it produces soil moisture as an output. The wind erosion scheme obtains friction velocity from the atmospheric model, soil moisture from the land surface scheme and land surface parameters from the GIS database. The wind erosion scheme predicts streamwise saltation flux and dust emission rate for different particle size groups. The transport and deposition model obtains flow velocity, turbulence data and precipitation from the atmospheric model and dust emission rate and particle size information from the wind erosion scheme. For the prediction, the atmospheric model and the land surface scheme are first run, followed by the wind erosion scheme, and then the calculations of dust transport and deposition are made.

[9] IWEMS as a whole and the dust emission, transport and deposition schemes are described by *Shao* [2001] and *Shao et al.* [2002]. These are briefly outlined here.

[10] The wind erosion scheme comprises three key parameterizations representing: (i) the wind erosion threshold friction velocity, u_{*t} [*Shao and Lu*, 2000]; (ii) the streamwise sand flux, Q [*Owen*, 1964]; and (iii) the dust emission rate F [*Shao*, 2001]. Dust particles are divided into I groups, each with a size d_i ($i = 1,\ldots,I$), and the dust emission rate for each group is predicted. Three dust emission mechanisms are considered: (1) aerodynamic lift; (2) saltation bombardment; and (3) aggregates disintegration. The dust emission rate for the ith group is expressed as

$$F(i) = F_a(i) + F_b(i) + F_c(i) \tag{1}$$

where F_a, F_b and F_c are dust fluxes respectively associated with the three mechanisms.

[11] $F(i)$ is an input for the dust transport scheme. Suppose the airborne dust concentration of the ith group is C_i, then the total airborne dust concentration is $C = \sum_i^I C_i$. The transport scheme predicts C_i (and hence C) by solving the dust conservation equation. In this study, we use six particle size groups: $d \leq 2$ μm, $2 < d \leq 11$ μm, $11 < d \leq 22$ μm, $22 < d \leq 40$ μm, $40 < d \leq 80$ μm and $d > 80$ μm. The reason for this classification of particle size groups is that the particle terminal velocity, which is involved in particle transport, should not vary excessively (more than a factor of 4) within each particle size group. Dust particles are delivered back to the surface by dry and wet deposition. Dry deposition is estimated using the scheme of *Raupach et al.* [2001]. Wet

deposition is not considered, but additional work is being carried out on this aspect.

[12] The area of simulation is (30°E, 5°N) to (180°E, 65°N) with a spatial resolution of 50 km. The area of data analysis is (72°E, 5°N) to (148°E, 53°N). In the vertical, the σ coordinate is used and the atmosphere is divided into 16 layers with smaller increments near the surface. The Atmosphere and Land Surface Interaction Scheme (ALSIS) is used for the simulation of land surface processes, including that of soil moisture [*Irannejad and Shao*, 1998].

[13] As our objective is to predict dust events in real time, we have nested IWEMS within the T213-GCM (Global Circulation Model), the operational model of the National Meteorological Centre of the China Meteorological Administration. The objective analysis of the T213-GCM is used for specifying the initial and boundary conditions for the atmospheric model of IWEMS, and the boundary conditions are updated every 6 hours using the forecasts of the T213-GCM. IWEMS is run continuously for March and April 2002. For each day, a 72-hour forecast is made, starting from 1200 UTC 1 March 2002. The atmospheric, land surface and dust fields are updated every few minutes, but all outputs are 3-hourly averages. At the beginning of each 72-hour forecast, the atmospheric variables (temperature, wind, humidity, etc.) are initialized using the T213-GCM objective analysis, while the dust variables are initialized using the predictions of the previous day.

[14] Land surface properties are specified using a set of parameters. The basic procedure of preparing these parameters is as described by *Shao et al.* [2002]. The wind erosion scheme mainly requires soil texture, vegetation type and vegetation cover as input data. On the basis of these data, the surface is divided into three basic categories: water, non-erodible and erodible lands. Dust emission is calculated only for erodible lands and in this case, the land surface data are used in the calculation of threshold friction velocity (u_{*t}) and dust emission.

[15] The calculation of u_{*t} requires roughness (mainly vegetation) frontal area index λ and soil moisture w as inputs. The former varies slowly with time and is assumed to be constant for a given location over a period of about two weeks. The latter experiences diurnal variations, responding to radiation, precipitation and other atmospheric and surface hydrological factors. Soil moisture is obtained from the ALSIS simulation for the top 50 mm soil layer. In this study, λ is derived from a combination of satellite NDVI (Normalized Differential Vegetation Index) data and vegetation-type data. For a given vegetation type, FPAR (fraction of photosynthetic active radiation) is estimated and an empirical relationship between λ and FPAR, either a linear, an exponential or a combination of linear and exponential functions, is then applied. The source of NDVI data is the NOAA/NASA Pathfinder AVHRR (Advanced Very High Resolution Radiometer) gridded data. Ten-day composite data mapped to the Goodes Homolosine projection with a resolution of 8 km are used for the work.

[16] The data sources for vegetation and soil types are LREIS (Laboratory of Resources and Environment Information System, Chinese Academy of Sciences), EOSDIS (Earth Observing System Data and Information System) and FAO/UNESCO (Food and Agriculture Organization/United Nations Educational, Science and Cultural Organization). The LREIS data, with a resolution of between 0.4 and 1.6 km, are limited to regions inside China. In this data set, vegetation in China is classified into 50 primary types. Soil in China is classified into 90 primary types. For regions outside China, EOSDIS vegetation data (1° resolution, 32 primary types) and the FAO/UNESCO soil data (0.5° resolution, 29 primary types) are used. The LREIS, EOSDIS and FAO/UNESCO data are merged to build a vegetation data set and a soil data set for the area of simulation, with soils reclassified into the 12 UNDA (the United States Department of Agriculture) soil texture classes and vegetation reclassified into 17 IGBP (International Geosphere-Biosphere Programme) vegetation types.

[17] The dust emission scheme requires minimally and fully dispersed particle size distributions, $p_m(d)$ and $p_f(d)$, as input quantities. Ideally, soil samples should be collected and analyzed to estimate $p_m(d)$ and $p_f(d)$ for each soil class. However, this type of data is not yet available for northeast Asia. To overcome this difficulty, $p_m(d)$ and $p_f(d)$ are regarded as a composite of several lognormal distributions [*Gomes et al.*, 1990; *Chatenet et al.*, 1996], e.g.,

$$p_m(d) = \frac{1}{d}\sum_{j=1}^{J}\frac{w_j}{\sqrt{2\pi}\sigma_j}\exp\left(-\frac{\left(\ln d - \ln D_j\right)^2}{2\sigma_j^2}\right) \qquad (2)$$

where J is the number of modes (typically 3), w_j is the weight for the jth mode of the particle size distribution, D_j and σ_j are parameters for the lognormal distribution of the jth mode. These parameters are obtained by fitting equation (2) to data particle size distribution estimated for Australian soils.

[18] The spatial resolution for dust prediction is determined by the resolution of the atmospheric model and that of the GIS data. In this study, the former is 0.5°. The GIS data sets, with various resolutions as described above, are formally unified at a spatial resolution of 0.05°, by applying spatial interpolation to lower resolution data and averaging to higher-resolution data. To increase the accuracy in the calculation of dust emission, the mosaic subgrid closure is used.

3. Synoptic Data

[19] The origin of northeast Asian dust storms is the arid and semiarid areas in northwestern China and southern Mongolia [*Zhou*, 2001; *Shao and Wang*, 2003]. The locations of the main deserts are indicated in Figure 1a, including (1) the Tagelamagen (Takla Makan); (2) the Zhunge'er (Junggar) Basin; (3) the Tulufan (Turpan) Basin; (4) the Chaidamu (Qaidam) Basin; (5) the Badanjilin (Badain Juran) and Tenggeli (Tengger) Sandy Desert; (6) the Wulanbu (Ulan Buh), Kubuqi (Hobq) and Maowusu (Mu Us) Sandy Desert; and (7) the Gobi Desert. The Gobi is about 2,000 km from east to west and about 1000 km from north to south.

[20] Surface weather records obtained through the meteorological networks are the best data available for establishing the climatology of northeast Asian dust events. Spread over the area defined by (70°E, 5°N) and (150°E, 55°N), there are approximately 1200 weather stations. At these stations, surface weather is recorded at 3-hourly intervals.

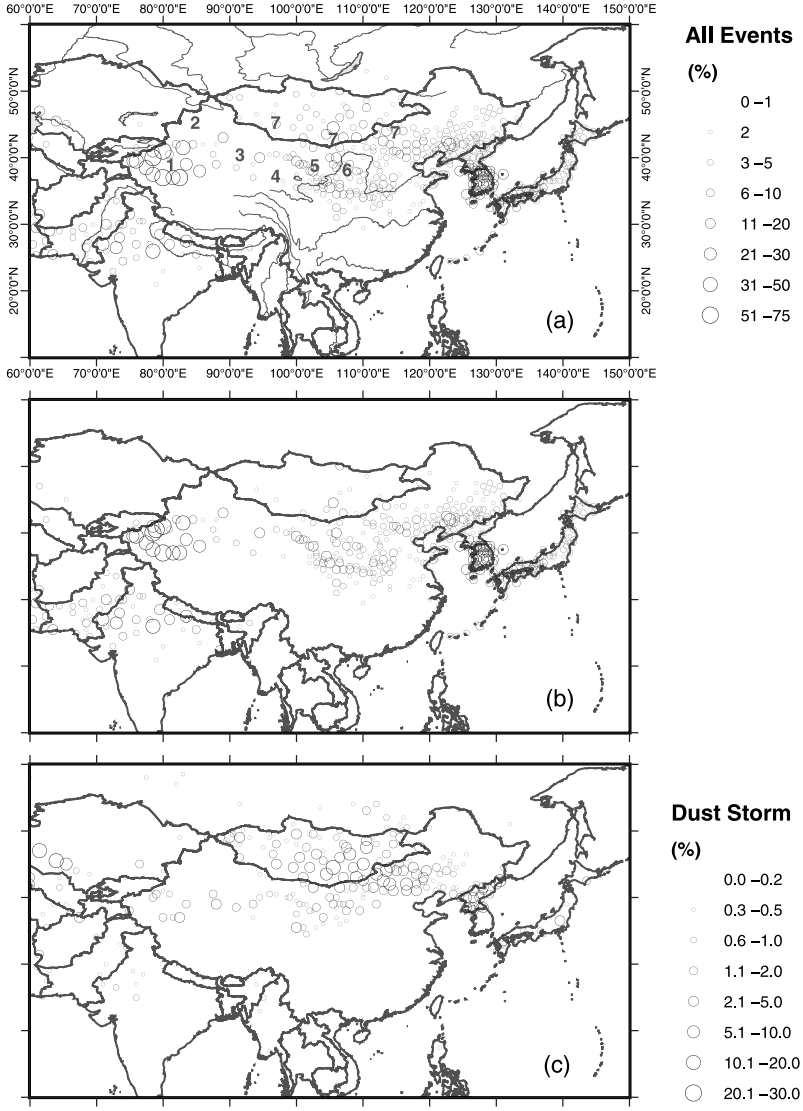

Figure 1. (a) Frequency of dust events, f_{DE}, for March, April, and May 2002, as observed by the meteorological network; (b) frequency of weak dust events, f_{WDE} (legend as in Figure 1a); and (c) frequency of strong dust events, f_{SDE}. In Figure 1a, the main deserts in northeast Asia are enumerated as follows: 1, Tagelamagan Desert; 2, Zhunge'er Basin; 3, Tulufan Basin; 4, Chaidamu Basin; 5, Badanjilin and Tenggeli Deserts; 6, Welanbu, Kubuqi and Maowusu Deserts; 7, Gobi Desert.

For a given observation time, the actual number of stations varied between 679 and 1545. In these records, dust events are classified into four categories according to horizontal visibility: (1) dust-in-suspension; (2) blowing dust; (3) slight to moderate sand-dust storm (dust storm hereafter); and (4) severe sand-dust storm (severe dust storm hereafter) [*Shao and Wang*, 2003].

[21] To facilitate discussion, we divide dust events into two categories, i.e., weak events including dust-in-suspension and blowing dust, and strong events including dust storms and severe dust storms. For a given location, we estimate the frequencies of the two categories, f_{WDE} and f_{SDE}, using weather records as follows:

$$f_{WDE} = N_{WDE}/N_{obs} \tag{3}$$

$$f_{SDE} = N_{SDE}/N_{obs} \tag{4}$$

where N_{WDE} and N_{SDE} are the number of observations of weak and strong dust events, respectively, and N_{obs} is the number of weather records. The frequency of occurrence of all dust events is

$$f_{DE} = f_{WDE} + f_{SDE}.$$

[22] Figure 1 shows the distributions of f_{DE}, f_{WDE} and f_{SDE} estimated using the surface weather records for March, April, and May 2002, for a region defined by (72°E, 5°N) and (148°E, 55°N). The following observations can be made: (1) Dust events are observed over a wide area of northeast Asia, including Mongolia, northwest, north, and northeast China, the Korean Peninsula and Japan. (2) The Talimu (Tarim) Basin, where the Tagelamagan is situated, is a region where dust events occur most frequently, with f_{DE} exceeding 50%. (3) The Gobi Desert in north-northeast

Table 1. Major Northeast Asian Dust Storms in March and April 2002

	Time	Class	Wind, m/s
1	3.15-17	DS	9-15 up to 20
2	3.18-22	SDS	9-15 up to 22
3	3.24-25	SDS	9-15
4	3.28-30	DS	9-15
5	3.30-31	DS	9-15
6	4.1-3	DS	7-12
7	4.5-9	SDS	9-15 up to 20
8	4.11	DS	7-12
9	4.13-17	DS	9-15 up to 22
10	4.19-20	DS	9-15 up to 22
11	4.21-24	SDS	9-15

China and South-Southeast Mongolia, is another region of frequent dust events. (4) A dusty belt, stretching from northwest to southeast along the Qilian Mountains (northeast of the Tibetan Plateau), can be identified. This dusty belt originates from the Badanjilin Desert to the north of Yumen (97°E, 40°N), elongating through the Tenggeli Desert, passing Xi'an (109°E, 34°N) and reaching Xinyang (114°E, 32°N). (5) The Indian Subcontinent is a region of frequent dust activities. Dust appears to travel along the southern boundary of the Tibetan Plateau.

[23] There are profound differences in the distributions of f_{WDE} and f_{SDE}. Figure 1c shows that most strong dust events occur in the Gobi Desert in Mongolia and Inner Mongolia. For other areas, the frequency of strong dust events is relatively low (high values of f_{SDE} in North Korea are probably due to observational bias). In particular, strong dust events only occasionally occur in the Talimu Basin. Figure 1b shows, in contrast, in the Talimu Basin weak dust events are the most frequent in northeast Asia.

[24] The prevailing synoptic system which generates northeast Asian dust events in March, April, and May is a low-pressure frontal system, referred to as the Mongolian Cyclone. The cyclone, accompanied by warm and cold fronts and a cutoff low or a deep trough at the 500 hPa level, is usually intense. Strong northwesterly winds prevail behind the cold front, generating dust storms or severe dust storms. Airborne dust particles are then transported by the northwesterly winds further down stream, affecting large areas in China, the Korean Peninsula and Japan. As a consequence, weak dust events (due to transported dust) are frequently reported in northeastern China, Korea and Japan (Figure 1b). Likewise, dust events over the Indian Subcontinent are mostly weak dust events.

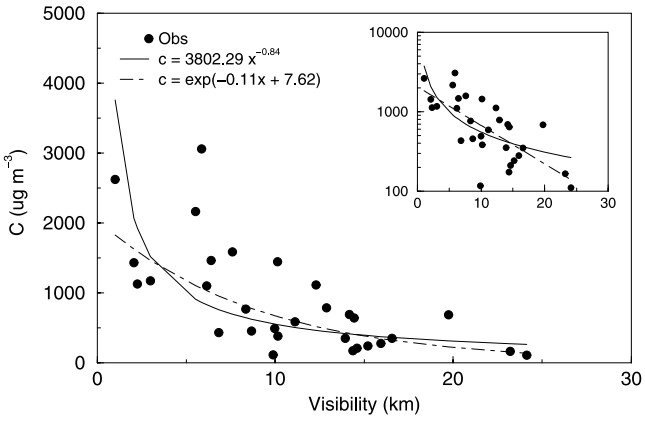

Figure 2. A plot of near-surface TSP measured using Andersen samplers versus visibility. Two different fittings are shown. The insert is the same as the main graph but with C in logarithmic scale.

4. Validation

[25] Weather records show that dust events occurred almost every day between 15 March and 25 April 2002. According to the National Meteorological Centre of CMA, these events can be grouped into 11 dust episodes, including 4 severe dust storms and 7 dust storms (Table 1). Most of these episodes developed under the synoptic condition of a strong cold air flow associated with a Mongolian Cyclone.

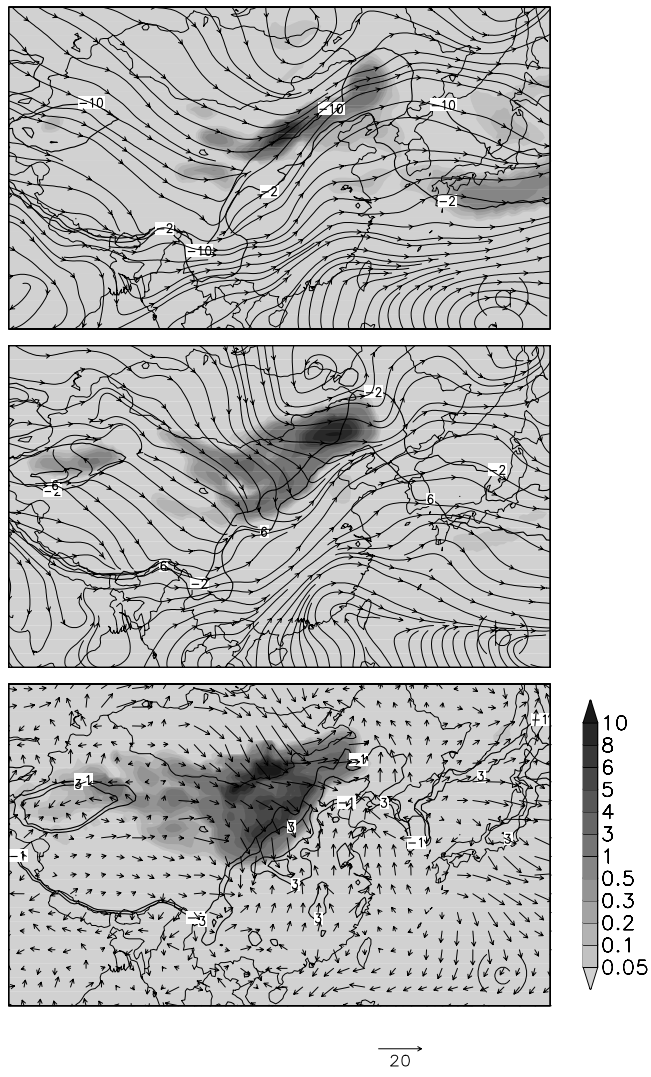

Figure 3. (a) Streamlines and dust concentration for σ = 0.7 for 0500 BST, 20 March (2100 UTC, 19 March) 2002; (b) as in Figure 3a, but for σ = 0.85 and (c) surface wind speed in ms^{-1} and dust concentration in $\mu g\ m^{-3}$. Note that in Figure 3a (and only in Figure 3a), dust concentration is enlarged by a factor of 5 for visualization. Also, in Figures 3a, 3b, and 3c, two isothermals are shown to indicate the location of the front.

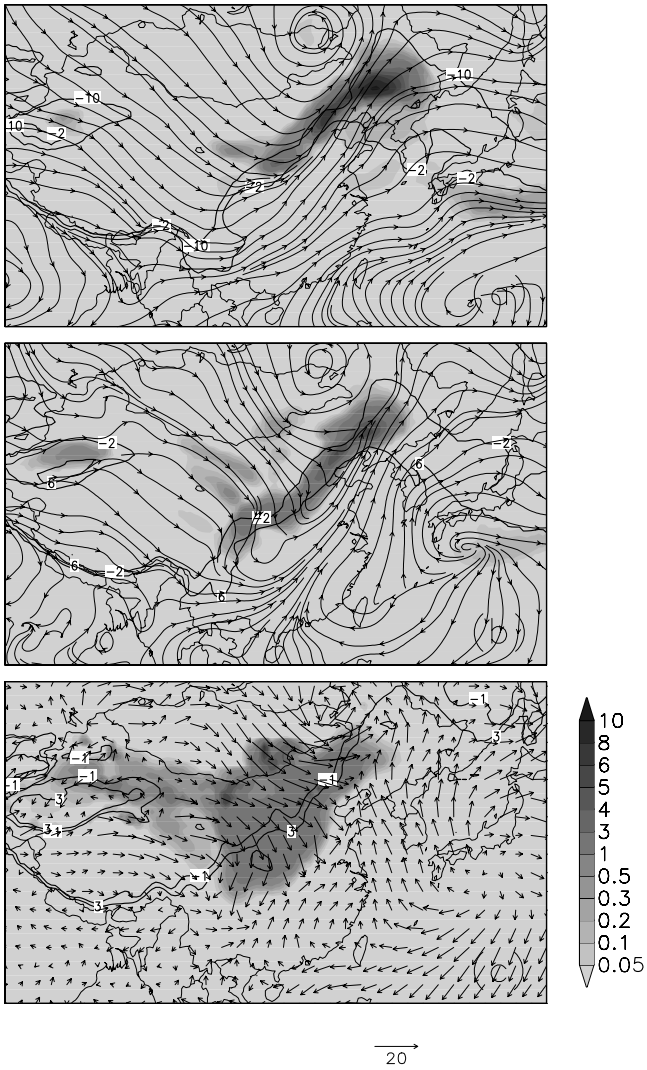

Figure 4. As Figure 3, but for 1100 BST, 20 March (0300 UTC, 20 March) 2002.

[26] The focus of this section is to verify the numerical predictions with observed data. Two data sets are used for the purpose. One is the surface weather records from the meteorological network and the other is the measurements of near-surface dust concentration at 12 stations spread across China, Japan and Korea. TOMS (NIMBUS 7 Total Ozone Mapping Spectrometer) is another likely source of data for comparison. However, for the region and time period considered, TOMS data are of poor quality and have to be discarded [see also *Prospero et al.*, 2002].

4.1. Validation With Synoptic Data

[27] The data set of weather records provides an excellent spatial and temporal coverage of dust activities As mentioned earlier, there are approximately 1200 weather stations at which weather observations are made at 3-hourly intervals. This data set is therefore most suitable for a qualitative comparison with the predictions in terms of spatial patterns and temporal development of dust activities.

[28] In the data set, apart from reports of dust events categories, visibility is also recorded. Visibility is mainly affected by the presence of aerosols and water vapor in the atmosphere. However, during a dust episode, it is reasonable to assume that aerosol plays a determining role and it is possible to estimate dust concentration from visibility using an empirical relationship. For Australia, G. H. McTainsh (personal communication, 2001) used the following relationship:

$$C = a/\sqrt{D_v} \tag{5}$$

where C is dust concentration in $\mu g\ m^{-3}$, D_v is visibility in km and a is a constant taken to be 400. In this study, we estimated a similar relationship for northeast Asia by fitting the near-surface TSP (Total Suspended Particle) measurements of Andersen samplers to visibility. Figure 2 shows the results. Despite the large scatter, a reasonable relationship between TSP and visibility exists: TSP rapidly increases with decreasing visibility. Using the least squares method, two likely empirical relationships are found, with respective correlation coefficient being 0.68 and 0.72,

$$C = 3802.29 D_v^{-0.84} \tag{6}$$

$$C = \exp(-0.11 D_v + 7.62) \tag{7}$$

While equation (7) fits to the bulk of the data better, equation (6) appears to be more reasonable for the range of very low visibility. We therefore use equation (6) for cases of $D_v < 3.5$ km, and equation (7) for cases of $D_v \geq 3.5$ km.

[29] In equations (6) and (7), the impact of air moisture on visibility is not included and the uncertainties in the empirical coefficients are large. However, for the purpose of this study, they remain very useful. In the comparisons to follow, we have used these expressions to convert visibility to dust concentration.

4.1.1. Dust Episode of 19–22 March 2002

[30] Synoptic records show that during 19–22 March 2002, severe and extensive dust storms successively affected Xingjiang, Qinghai, Gansu, Inner Mongolia, Ningxia, Shaanxi, Shanxi, Hebei, Beijing, Tianjin, Liaoning, Jilin, Heilongjiang, Shandong, Henan, Hubei, Hunan, and Sichuan. Severe dust storms occurred in Inner Mongolia, Gansu, Ningxia, Hebei, Beijing, and Jilin. Zero visibility were reported at Dingxing (Gansu) and Wulate-Houqi (Inner Mongolia). At the late stages of the episode, the Korean Peninsula and Japan were affected. In South Korea, high dust concentrations were recorded on 21 and 22 March, and schools were closed on these days.

[31] The weather condition which resulted in this dust episode is depicted in Figures 3 and 4, in which the predicted flow and dust concentration fields for 0500 and 1100 BST, 20 March 2002, are shown (BST = UTC + 8 hours is Beijing Standard Time). A deep trough over Mongolia dominated the synoptic situation in northeast Asia. At the surface, very strong winds occurred in the cold regime of a cyclone, with maximum wind speed exceeding 20 ms^{-1}, causing severe dust storms behind the cold front. Dust particles were confined to the region behind, with the highest dust concentration occurring in the vicinity of, the cold front. In subsequent hours (Figure 4), dust storms moved eastward, corresponding to the eastward motion of the cyclone and the regime of strong northwesterly wind.

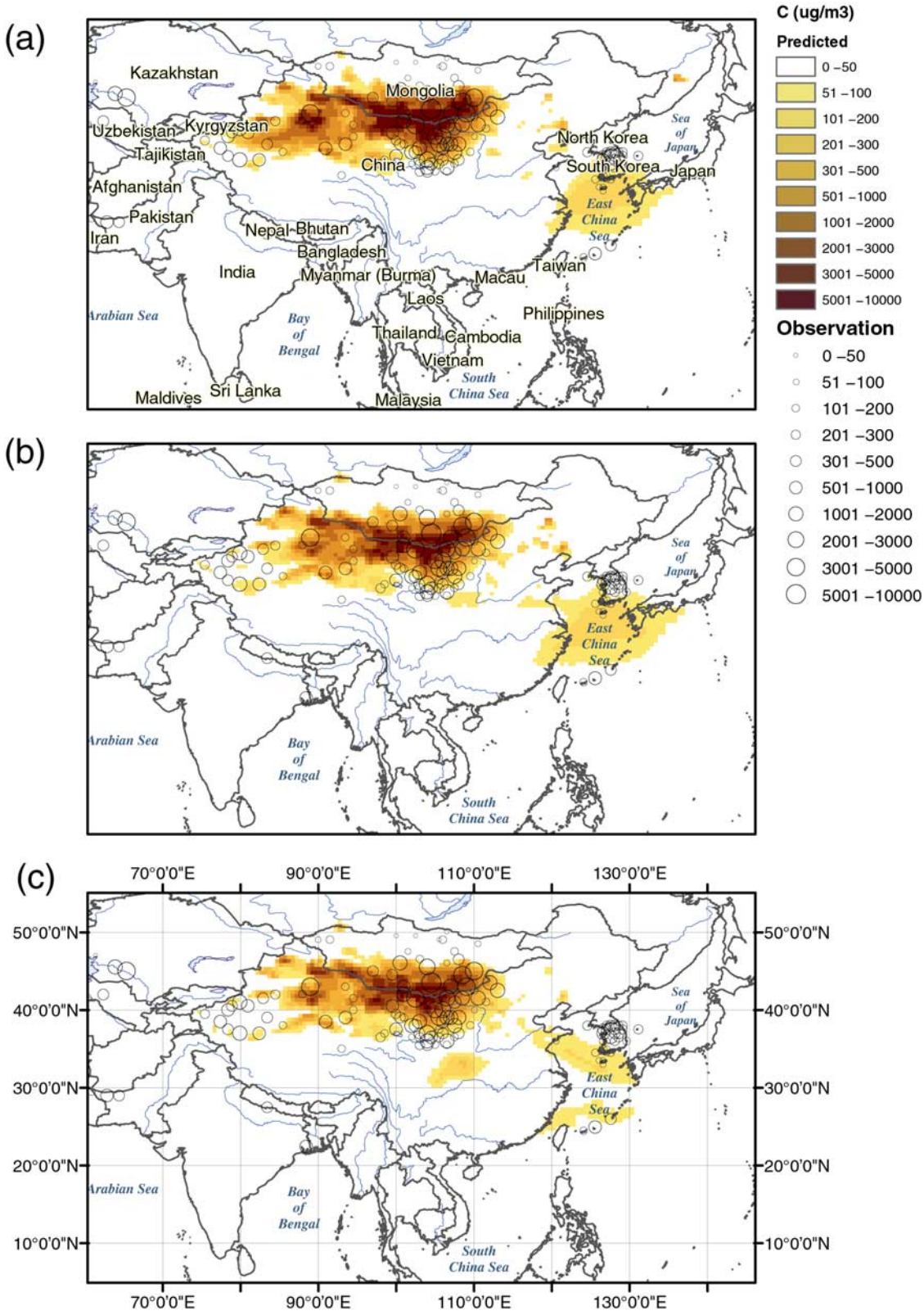

Figure 5. Comparisons of the predicted and observed near-surface dust concentration for 19 March. (a) the 24-hour forecast; (b) the 48-hour forecast; and (c) the 72-hour forecast. Circles represent the stations where dust events were observed, and the sizes of circles represent the magnitude of dust concentration.

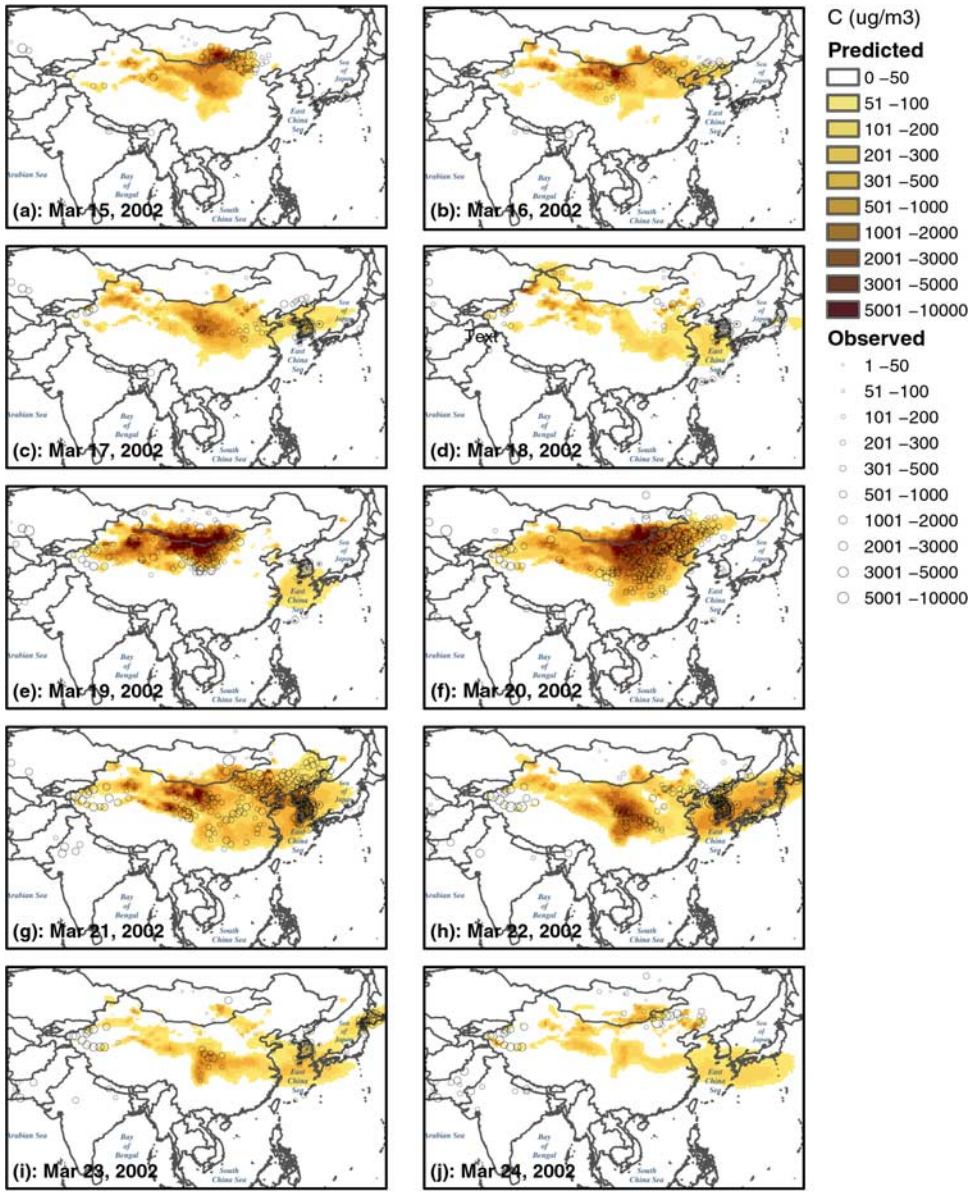

Figure 6. (a–j) Comparisons of the predicted and observed near-surface dust concentration (in $\mu g\ m^{-3}$) for 10 successive days from 15 to 24 March 2002. The model results are the 24-hour forecasts.

[32] In Figure 5, the predicted and observed near-surface dust concentrations for 19 March are compared. The 24-, 48-, and 72-hour forecasts are shown together with the observations (dust concentration derived from equations (6) and (7)). Both the predictions and the observations are averages over the period between 2300 BST, 18 March, and 2300 BST, 19 March 2002, i.e., the 24-, 48-, and 72-hour forecasts are the averages over this period obtained from the model runs starting from 2000 BST, 18 March, 2000 BST 17 March, and 2000 BST, 16 March, respectively.

[33] Figure 5 shows that the agreement between the predicted and observed dust concentration is excellent in terms of spatial pattern and intensity. The model successfully predicted the severe dust storms occurred along the China-Mongolia border, centered at about (105°E, 42°N). Some detailed aspects of the episode were also correctly predicted. For instance, the predicted high dust concentration in the Tulufan Basin (in the vicinity of (89°E, 43°N)) coincides well with the observations there and the predicted dust clouds over the East China Sea are confirmed by the observations at the nearby stations in South Korea and Japan. The dust activities reported in Kazakhstan and Pakistan were not correctly predicted, because of the poor land surface data used for these regions. This indicates, from a different perspective, the importance of land surface data to the prediction of dust events. Figure 5 also shows that the 48- and 72-hour forecasts are of high quality. Only small differences can be detected in the 24-, 48-, and 72-hour forecasts for this dust event.

[34] In Figure 6, successive forecasts of near-surface dust concentration for the 10 day period between 15 and 24 March 2002 are compared with observations. The figure demonstrates that the modeling system well predicted the

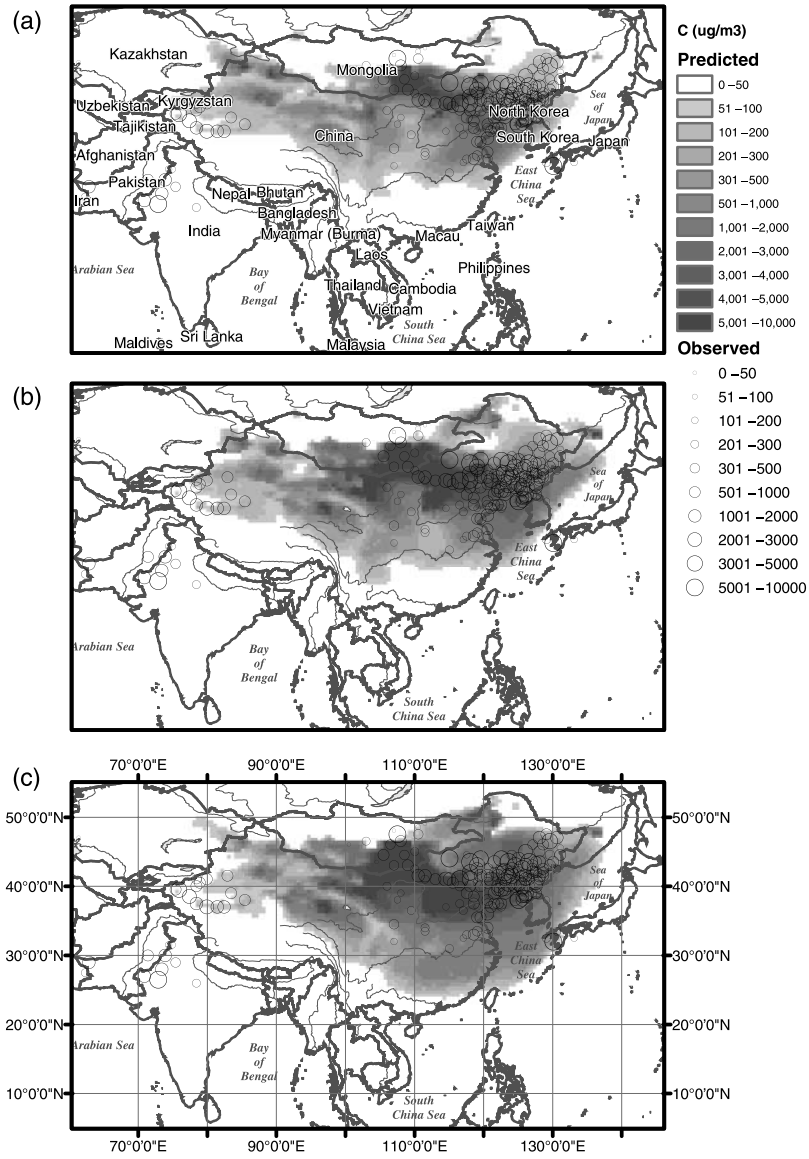

Figure 7. As in Figure 5, but for 7 April 2002.

spatial distributions and temporal evolutions of all dust events in this period of time. The dust episodes are well identified. For example, the 19–22 March episode first developed on 19 March in the Gobi Desert near the China-Mongolia border. Near the center of the dust storm (in the vicinity of (105°E, 42°N)), both the predicted and the observed near-surface dust concentration exceeded 10,000 $\mu g\ m^{-3}$. In the next two days, the center of the dust storm moved eastward and dust activities became widespread, but the near-surface dust concentration was generally decreasing. By 21 March, dust clouds covered a large part of China and the entire Korean Peninsula and the dust front reached Japan. By 22 March, both model prediction and observation showed a dust band stretching several thousands of kilometers. A large part of China, the entire Korean Peninsula and entire Japan were under the influence of dust clouds with quite high concentration. The dust storm was much weaker by 23 March, with dust concentration falling below 500 $\mu g\ m^{-3}$ in most places. The dust episode probably ended around 24 March. On this day, the residual of the dust storm can be seen and the dust concentration was generally below 200 $\mu g\ m^{-3}$. As can also be seen from Figure 6, 15 to 19 March 2002 can be considered as another episode.

4.1.2. Dust Episode of 5–9 April 2002

[35] In April 2002, six dust episodes were observed one following the other. The 5–9 April episode was the most severe. As Figure 7 shows, the predictions and the observations are in general agreement. In particular, the high dust concentration observed in the eastern part of China were correctly predicted. A disagreement can be detected for the western part of China (around 95°E, 40°N), where a significant dust concentration was predicted, while no dust activities were reported except for the Talimu Basin. Some uncertainties exist in this comparison, because there are relatively few weather stations in this region and the synoptic dust reports are sometimes unreliable (neither the TOMS data showed dust activities in this region, however,

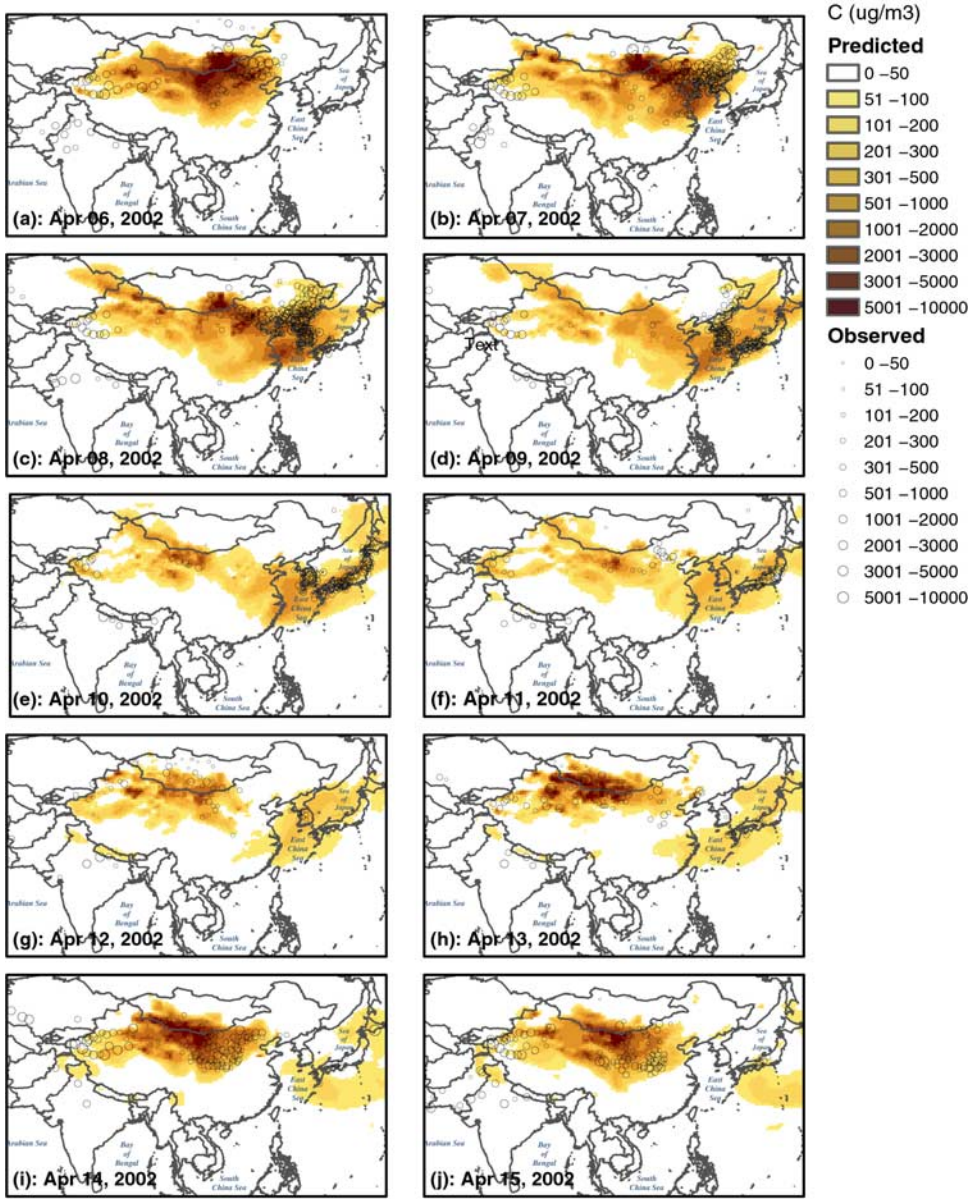

Figure 8. As in Figure 6, but for the time period from 6 to 15 April 2002.

the TOMS data are known to be unreliable for this part of the world, as a comparison of synoptic records and TOMS data would reveal). Among the three forecasts, there is a qualitative agreement in the tendency of dust storm development, but the 48-hour and the 72-hour forecasts are too strong, especially the latter, both in terms of intensity and extent. We believe that this is mainly due to the error growth in the atmospheric component of the modeling system, which typically increases with time. For the particular event, the intensity of the low-pressure system and the strength of near-surface winds were over predicted. However, Figure 7 also reveals a positive aspect of the modeling system, that is, the quality of the forecast improved as the period of forecast became shorter, as a comparison of the 24-, 48-, and 72-hour forecasts confirms: the 24-hour forecast was in much better agreement with the observations when compared with the 48- and 72-hour forecasts.

[36] Similar to Figure 6, the successive forecasts of near-surface dust concentration for the 10 day period between 6 and 15 April 2002 are compared with observations in Figure 8. Again, the modeling system well predicted the dust activities for this period of time. The 5–9 April strong episode, the 10–11 April weak episode and the 13–17 April episode of medium strength are all well predicted. Comparing the 19–22 March and the 5–9 April episodes, we observe similar features in the development of dust storms in northeast Asia. Again, the Gobi Desert near the China-Mongolia border was the main source region of dust. However, for the 5–9 April episode, it was located further to the east, around (110°E, 42°N). Near the center of the dust storm, both model predicted and observed near-surface dust concentration exceeded 10,000 $\mu g\ m^{-3}$ (for some small areas, the model prediction was more than 20,000 $\mu g\ m^{-3}$). On 6 April 2002, the center of the dust

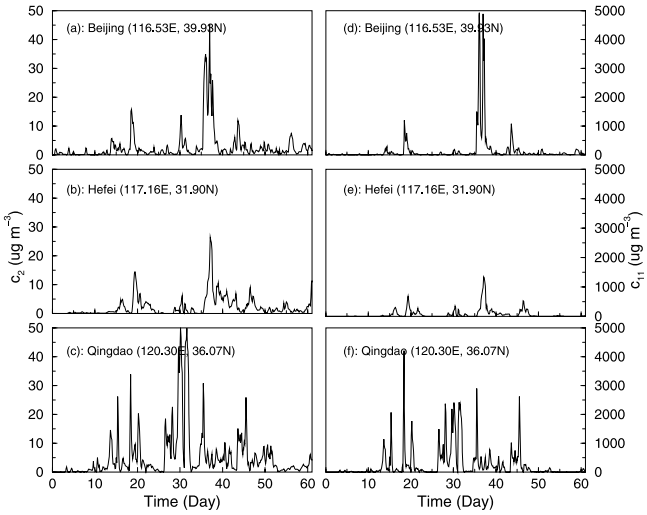

Figure 9. (a–f) Predicted daily averages of $c_{2\mu}$ and C_{11} for Beijing, Hefei, and Qingdao for March and April 2002. The starting date is 1 March 2002. See Table 2 for the geographic positions of the stations.

clouds was in the vicinity of (110°E, 42°N). The dust clouds subsequently moved eastward, affecting the northeast part of China, the Korean Peninsula and Japan.

4.2. Validation With Point Observations: China and Japan

[37] Near-surface dust concentration has been measured at a number of locations in northeast Asia. We use the measurements taken at 11 stations for comparison with model predictions. Nine of the stations are located in or downstream of the dust source regions, with 5 in China (Dunhuang, Shapotou, Beijing, Hefei, and Qingdao) and four in Japan (Fukuoka, Nagoya, Tsukuba, and Naha). Two of the stations (Cele (Qira) and Akesu (Aksu)) are located in the Talimu Basin. To facilitate discussion, we separate the 11 stations into three groups: the East Group including Beijing, Qingdao, Hefei, Fukuoka, Nagoya, Tsukuba, and Naha, the West Group including Dunhuang and Shapotou, and the Talimu Group including Cele and Akesu. At these locations, dust concentration were measured using low-volume Andersen samplers AN-200 (Shibata Scientific Co. Ltd), mounted mostly on roof tops. The flow rate was maintained at 28.3 liters per minute. AN-200 uses eight stages for particle size discrimination (>11, 11-7.0, 7.0-4.7, 4.7-3.3, 3.3-2.1, 2.1-1.1, 1.1-0.65, and 0.65-0.43), as well as a backup filter. The filters used are as follows: PF050 ployflon filters for stages 0–6 (Advantec Co. Ltd.) and 2500QAT-UP quartz filters for stage 7 and the backup (Tokyo Dylec Co. Ltd.). The filters was kept in a desiccator before and after sampling. The weight of the filter was measured before and after sampling, and the dust concentration in the air was calculated by dividing the weight difference by air volume [*Yabuki et al.*, 2002; *Kanai et al.*, 2002]. For these 11 stations, C_{TSP}, C_{11} and C_2 are used for comparison, which are respectively the concentration of all particles, that of particles smaller than 11 μm and that of particles smaller than 2.1 μm.

[38] Figure 9 shows the predicted daily averages of C_2 and C_{11} for Beijing, Hefei and Qingdao for March and April 2002. Several observations can be made on the basis of Figure 9: (1) dust concentration at the three locations vary considerably with time, showing clearly higher values during dust episodes. For instance, C_{11} reached 5000 μg m^{-3} and C_2 reached 45 μg m^{-3} in Beijing during the 5–9 April dust episode; (2) the orders of magnitude of C_2 and C_{11} for these stations are around 10 and 10^3 μg m^{-3} during dust episodes; and (3) dust concentration is much lower in Hefei than in Beijing and Qingdao, an indication that the movement of dust particles has preferred trajectories.

[39] Figure 10 shows the predicted daily averages of C_2 and C_{11} for Fukuoka, Nagoya, Tsukuba and Naha. A comparison of Figures 10 and 9 confirms that dust concentrations at the Japanese stations are clearly lower, as expected. However, Fukuoka, located closer to the Eurasia continent, is strongly affected by transported dust. For example, C_{11} reached 1500 μg m^{-3} and C_2 reached 40 μg m^{-3} in Fukuoka on 9 April 2002. The other three Japanese stations showed lower values, but the dust signals are clearly identifiable. For example, the 5–9 April dust episode occurred on the continent elevated the dust concentration in Nagoya and Tsukuba to levels between 100 and 300 μg m^{-3}. Even at Naha, located at (127.7°E, 26.2°N), the dust signals remain visible, although much weaker.

[40] In Figures 11 and 12, C_{TSP}, C_{11} and C_2 observed over various time periods in March and April 2002 are compared with the corresponding predictions for 9 stations of the East Group and the West Group (the Talimu Group is excluded here, but discussed later). The predictions are the averages over the same time period as the observations, and over 9 grid cells surrounding the station and over three layers in vertical (σ = 0.999, 0.998 and 0.995).

[41] We first consider C_{TSP}, represented by the open symbols in Figure 11. Clearly, there is a good agreement between the predictions and the observations. However, for the East Group (apart from Qingdao, Table 2), the predicted values are generally smaller than the observed ones. It is

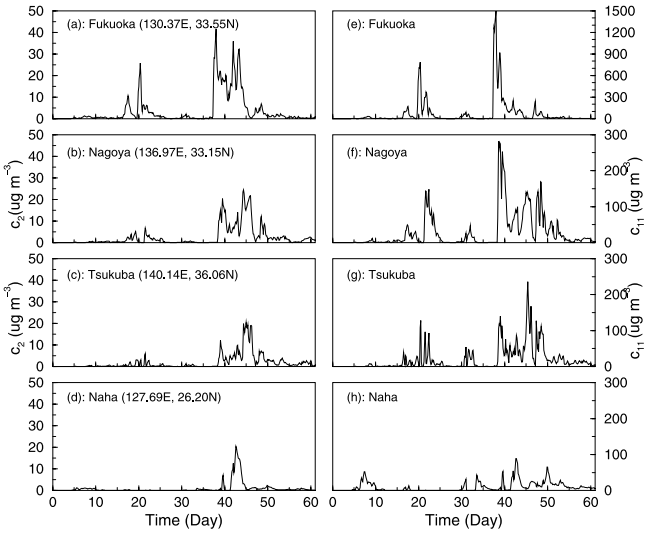

Figure 10. Same as Figure 9, but for Fukuoka, Nagoya, Tsukuba, and Naha.

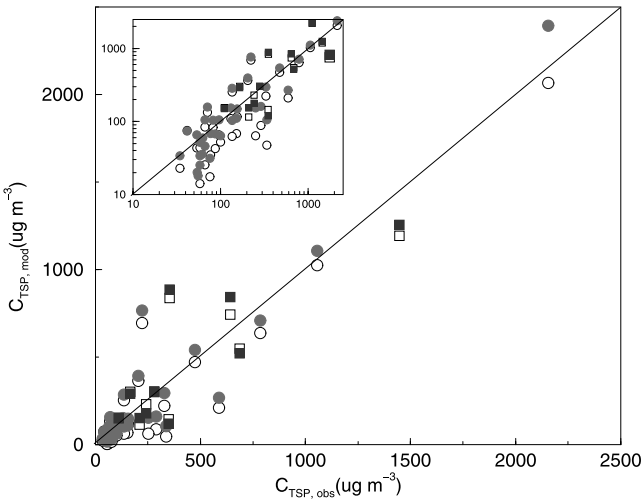

Figure 11. A comparison of predicted and observed TSP for the East Group (open circles) and for the West Group (open squares). The solid circles and solid squares represent $\hat{C}_{TSP}$ obtained using equation (8). The insert is the same as the main graph but in logarithmic scales.

important to note that while Dunhuang and Shapotou (the West Group) are located in the vicinity of deserts in western China where airborne particles are primarily natural dust, the other seven stations (the East Group) are located in eastern China and Japan where airborne particles originate both from natural and anthropogenic sources.

[42] The predicted and the observed C_2 disagree (Figure 12b), with the former being much smaller, almost by an order of magnitude. The disagreement is most obvious for the East Group stations (Table 2). This is not unexpected. A size distribution analysis of the particles collected by the Andersen samplers reveals that most samples have a bimodal size distribution with one peak at around 0.5 μ and the other at around 5 μ. When dust events occur, the concentrations of the coarser particles clearly increase and hence it is certain that these increases are due to aeolian dust. The former peak (smaller than 2.1 μm) is most likely associated with particles of anthropogenic origin. It can be shown through the chemical analysis of the samples that particles of anthropogenic origin consist mostly of carbon and ammonium sulfate. Indirect supporting evidence is that dust concentration is low in Japan compared to China, so the Andersen samplers must be operated for longer periods (4–7 days during intensive observation periods and 14–20 days for a normal measurement) to ensure an identifiable filter weight difference before and after sampling. Thus, in terms of sampling duration, the measurements are biased toward background aerosols which are not necessary aeolian.

[43] On the basis of the above discussions, we introduce

$$\hat{C}_{TSP,mod} = C_{TSP,mod} - C_{2,mod} + C_{2,obs} \tag{8}$$

$$\hat{C}_{11,mod} = C_{11,mod} - C_{2,mod} + C_{2,obs}. \tag{9}$$

We have also plotted $\hat{C}_{TSP,mod}$ and $\hat{C}_{11,mod}$ against $C_{TSP,obs}$ and $C_{11,obs}$ in Figures 11 and 12. As can be seen, there is an improved agreement between the predicted and observed dust concentrations. The correlation coefficient is 0.91 for C_{TSP} and 0.77 for C_{11}.

[44] For the Talimu Basin, observations were available only for Cele and Akesu. Cele is located at the southern fringe of the basin, while Akesu is at the northwestern. The comparison between the predicted and the observed dust concentration for these two stations is poor, as summarized in Table 3. In particular, the model failed to predict the dust storms observed at Cele during 15–17 April 2002 and at Akesu on 5, 13, 20, and 22 April 2002. While this failure requires further investigation, two possible reasons are: (1) The flow pattern within the Talimu Basin is complicated by the presence of high mountains surrounding it and the mountain-basin wind system which is quite prominent for Cele and Akesu. It cannot be ruled out that the above-mentioned dust storms were generated by localized strong winds which the atmospheric model cannot predict; (2) In the wind erosion model, the rate of dust emission is related to soil type. For example, dust emission from a sand surface would be low regardless of wind intensity, because the percentage of fine particles in sand is small. In this study, we classified the Tagelamagan as a sandy desert. This is probably far from the true surface condition of the basin. Improved soil data will be used in future studies.

4.3. Validation With Point Observations: South Korea

[45] In addition, TSP time series observed at Mount Gwanak (126.97E, 37.44N, South Korea) are compared

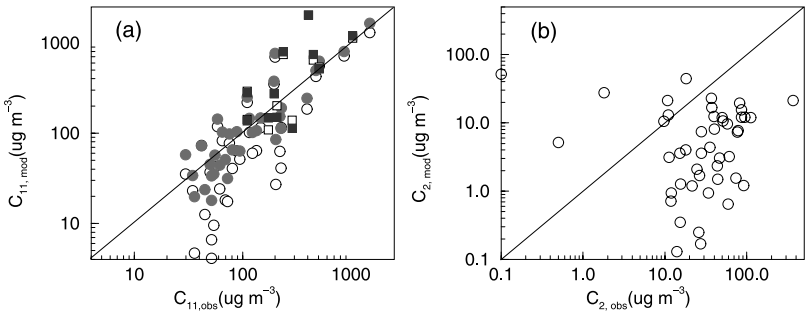

Figure 12. (a) A comparison of predicted and observed C_{11} for the East Group (open circles) and for the West Group (open squares). The solid circles and squares represent C_{11} modified using equation (9). (b) A comparison of observed and predicted C_2.

Table 2. Comparison of Observed and Predicted C_{11} and C_2 for Nine Stations for Various Time Periods in March and April 2002[a]

Start Time	End Time	$C_{TSP,obs}$	$C_{11,obs}$	$C_{2,obs}$	$C_{TSP,mod}$	$C_{11,mod}$	$C_{2,mod}$	$\hat{C}_{TSP,mod}$	$\hat{C}_{11,mod}$
				Beijing (*116.53°E, 39.93°N*)					
19 March 0200	21 March 0200	1056.39	867.44	94.47	1024.29	718.00	12.10	1106.66	800.37
8 April 0100	8 April 1300	1464.64	988.38	261.18	2004.37	1272.62	20.38	2245.17	1513.42
11 April 1000	14 April 0500	691.01	506.48	106.01	41.90	21.15	0.84	147.07	126.32
14 April 0500	15 April 0500	785.24	510.40	78.52	638.55	553.81	7.70	709.37	624.63
15 April 0700	16 April 0700	588.93	392.62	61.35	211.04	184.80	3.20	269.19	242.95
16 April 0800	17 April 0200	337.00	202.85	58.89	47.29	27.04	0.65	105.53	85.28
17 April 0200	19 April 0200	289.56	226.98	73.62	88.56	41.10	1.55	160.63	113.17
21 April 0100	22 April 0100	328.82	228.21	85.89	221.78	115.49	12.10	295.57	189.28
				Hefei (*117.16°E, 31.90°N*)					
15 March 0800	20 March 0800	152.42	134.38	44.21	68.50	63.85	1.49	111.22	106.57
21 March 0700	28 March 0200	136.34	123.07	43.67	62.48	60.11	2.34	103.81	101.44
30 March 1100	5 April 0800	252.20	220.78	91.23	63.68	62.96	1.21	153.70	152.98
12 April 0100	19 April 0700	131.00	116.14	46.59	109.06	101.97	3.05	152.60	145.51
				Qingdao (*120.30°E, 36.07°N*)					
8 March 0300	14 March 0300	77.30	69.53	33.95	34.95	18.17	0.94	67.96	51.18
20 March 0300	23 March 0200	473.61	473.61	76.60	471.79	423.29	7.35	541.04	492.54
1 April 0800	4 April 0700	223.13	199.90	86.27	695.28	692.54	15.63	765.92	763.18
8 April 1100	13 April 0700	135.83	110.58	35.35	254.43	219.77	4.41	285.37	250.71
15 April 0500	19 April 0800	70.79	58.89	27.96	133.89	118.81	3.59	158.26	143.18
				Fukuoka (*130.37°E, 33.55°N*)					
1 March 0300	22 March 0200	87.24	80.21	26.46	42.59	40.67	1.70	67.35	65.43
22 March 0700	5 April 1000	62.68	55.45	15.52	45.29	42.78	1.27	59.54	57.03
6 April 0000	11 April 0700	204.34	194.04	39.67	365.56	349.81	12.42	392.80	377.06
12 April 0200	16 April 0300	66.61	64.97	37.55	84.10	82.33	16.67	104.98	103.21
17 April 0100	15 April 0000	53.63	29.75	24.52	43.55	35.20	2.10	65.97	57.62
25 April 0000	10 April 0900	27.57	19.69	12.06	NA	NA	NA		
				Nagoya (*136.97°E, 33.15°N*)					
18 March 0700	2 April 0300	66.49	61.40	21.53	25.51	24.06	1.20	45.84	44.39
2 April 0800	8 April 0000	58.09	51.93	27.28	6.76	6.60	0.17	33.87	33.71
8 April 0100	12 April 0400	155.31	146.30	40.27	116.73	115.55	8.14	148.86	147.68
12 April 0600	15 April 0600	96.10	88.32	50.93	65.33	63.67	10.72	105.54	103.88
16 April 0700	21 April 0200	82.25	75.64	27.86	83.56	77.17	7.46	103.96	97.57
				Tsukuba (*140.14°E, 36.06°N*)					
1 March 0500	20 March 0100	54.05	35.90	15.37	5.10	4.69	0.35	20.12	19.71
20 March 0800	1 April 0400	58.50	44.77	11.90	14.11	12.56	0.71	25.30	23.75
1 April 0600	8 April 0500	61.89	54.12	25.82	9.96	9.54	0.25	35.53	35.11
8 April 0500	12 April 0500	100.06	94.31	15.26	52.14	51.45	3.59	63.81	63.12
12 April 0500	17 April 0100	41.74	41.74	9.68	75.05	73.33	10.58	74.15	72.43
17 April 0200	24 April 0200	58.45	50.15	11.21	43.84	37.07	3.13	51.92	45.15
				Naha (*127.69°E, 26.20°N*)					
18 March 0800	6 April 2200	55.32	51.65	14.04	4.13	4.11	0.13	18.04	18.02
7 April 0100	16 April 2200	76.05	72.73	17.94	17.49	17.46	4.03	31.40	31.37
16 April 2400	24 April 0800	34.50	34.50	12.02	22.98	22.98	0.94	34.06	34.06
				Shapotou (*104.95°E, 37.50°N*)					
10 April 0400	12 April 0200	642.51	447.90	112.01	743.80	643.00	12.00	843.81	743.01
15 April 0300	15 April 0800	1115.81	405.08	37.02	2212.39	2016.01	23.03	2226.38	2030.00
16 April 0300	18 April 0200	353.11	237.66	57.91	836.99	743.94	9.60	885.30	792.25
18 April 0200	20 April 0200	210.36	173.29	50.13	114.98	108.34	11.90	153.21	146.57
				Dunhuang (*80.78°E, 37.02°N*)					
7 April 0400	9 April 0100	687.48	509.31	1.81	547.87	538.08	27.59	522.09	512.30
9 April 0300	11 April 0100	279.78	196.37	10.98	303.32	274.56	13.09	301.21	272.45
11 April 0200	3 April 0100	110.41	110.41	0.50	154.93	141.22	5.19	150.24	136.53
13 April 0200	14 April 0100	1447.75	1039.99	81.86	1192.43	1130.50	19.54	1254.75	1192.82
14 April 0200	17 April 0100	165.81	109.99	10.78	302.02	289.94	21.13	291.67	279.59
17 April 0200	19 April 0800	348.70	285.68	18.19	145.89	138.57	44.33	119.75	112.43
19 April 0800	21 April 0200	241.30	207.02	0.00	230.04	201.71	51.59	178.45	150.12

[a]Times are given in UTC. C_{11} and C_2 are near-surface dust concentrations of particles smaller than 11 μm and 2 μm, respectively.

with the model predictions for the time period of 21–22 March and 8–9 April. The height of Mount Gwanak is 629 m above sea level, located in the vicinity of Seoul. In Figure 13, the time series of the observed and the predicted TSP for Mount Gwanak are shown. As can be seen, the predicted and the observed TSP evolution are in agreement for both cases. For 21–22 March, the predicted peak value of TSP is somewhat lower that the observed and the second

Table 3. Comparison of Observed and Predicted Dust Concentrations for Cele (80.78°E, 37.00°N) for the Period 9–18 April 2002 and for Akesu (80.25°E, 41.17°N) for the Period 1–24 April 2002[a]

	IOP-1	IOP-2	IOP-3	IOP-4	IOP-5	IOP-6	IOP-7	IOP-8
				Cele				
Start time	9 April 0300	10 April 0400	11 April 0100	12 April 0100	14 April 0900	15 April 0200	16 April 0100	17 April 0100
End time	10 April 0300	11 April 0100	12 April 0100	14 April 0800	15 April 0200	16 April 0100	17 April 0100	18 April 0100
$C_{2,obs}$	31.32	46.20	12.81	8.19	38.78	58.46	75.09	71.42
$C_{11,obs}$	348.22	315.56	116.81	314.04	2143.76	1035.13	893.41	796.93
$C_{TSP,obs}$	433.13	456.32	116.81	491.93	2621.56	1432.65	1130.08	1171.34
$C_{2,mod}$	3.60	4.00	5.84	6.27	33.48	33.48	32.67	18.50
$C_{11,obs}$	114.38	218.24	218.42	125.82	119.68	83.41	64.01	55.70
$C_{TSP,obs}$	128.06	250.80	237.60	144.29	131.79	91.24	68.06	60.50
				Akesu				
Start time	1 April 0500	5 April 0500	11 April 0100	13 April 1000	17 April 0800	20 April 0800	22 April 0500	
End time	4 April 0700	7 April 0800	13 April 0600	16 April 2100	20 April 0300	22 April 0100	24 April 0800	
$C_{2,obs}$	15.05	124.84	38.92	295.95	78.22	308.76	79.05	
$C_{11,obs}$	131.64	1361.71	302.89	1857.72	650.94	2631.90	908.30	
$C_{TSP,obs}$	173.20	1584.61	384.36	2165.86	767.61	3058.78	1101.72	
$C_{2,mod}$	1.63	5.16	4.32	4.63	9.68	2.48	9.07	
$C_{11,mod}$	73.90	146.22	142.34	106.32	79.25	108.74	230.77	
$C_{TSP,mod}$	84.73	158.23	161.52	72.27	89.76	124.18	237.80	

[a]Times are given in UTC, and concentrations are given in μg m^{-3}.

(minor) peak on 22 March was missing. Despite these minor differences, the agreement between the prediction and the observation is good.

5. Key Terms of Dust Budget

[46] In light of the comparisons presented above, it can be argued that IWEMS has the capacity to predict quantitatively the key terms of dust balance. In this section, we use the predictions to examine such key quantities as dust emission, dust load and deposition which so far are poorly understood.

[47] As an example, dust emissions for the four days between 18 and 21 March 2002 are shown in Figure 14, together with friction velocity (u_*) and observed dust concentration. Both dust emission and friction velocity are daily averages. It is seen that dust sources vary substantially in space and time, depending on the strength of winds (represented by u_*) and surface conditions (represented by u_{*t}. On 18 March, u_* was generally small and consequently, dust emission occurred only in isolated locations. On 19 March, wind speed strengthened significantly with u_* reaching 1 ms^{-1}, leading to strong dust emission from the Tulufan Basin, the Hexi Corridor and the Gobi Desert in southern Mongolia and Inner Mongolia. The maximum intensity of dust emission reached 5000 μg m^{-2} s^{-1}. Severe dust storms were reported on this day. On 20 March, dust emission weakened and the main region of dust emission was the eastern part of the Gobi. On 21 March, dust emission further weakened, confined to a smaller region in the Hexi Corridor and parts of the eastern Gobi. There were only very weak dust emissions on 22 March.

[48] The cumulative net dust flux for the simulation period can be estimated as follows:

$$F_{net} = \int_0^T (F - D)dt \qquad (10)$$

where F and D are dust emission and deposition, respectively, and T is time span (March and April 2002 in our case). Figure 15 shows the results. The regions of net positive dust flux (source) are mainly the deserts in inland China and southern Mongolia. These include the fringes of the Talimu Basin, the western part of the Zhunge'er Basin, the Tulufan Basin, the Chaidamu Basin and the Gobi Desert. Positive net dust flux is also predicted for isolated locations along the southeastern fringes of the Gobi Desert. The Gobi Desert has by far the strongest net dust emission, reaching 1000 t km^{-2} over the March–April period. The Talimu Basin did not appear as a strong dust source for this time period. There are uncertainties in this statement, but it appears to be consistent with the study of *Shao and Wang* [2003] and with the fact that intensive dust events did not occur until late April in 2002.

[49] Net negative dust flux (sink) covers a wide area. Large parts of China, the Korean Peninsula and Japan

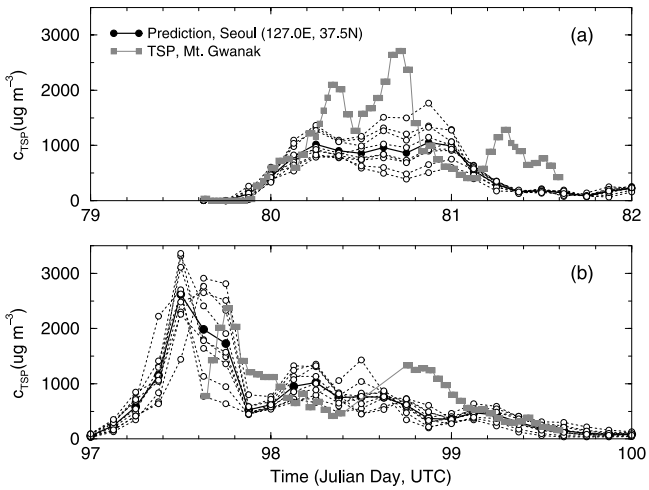

Figure 13. (a and b) A comparison of the observed and predicted time series of TSP for Mount Gwanak. Predicted TSP (d < 22 μm) from 9 grid cells adjacent to Seoul are shown (open circles) together with their average (solid circles). The measurements are shown as solid squares.

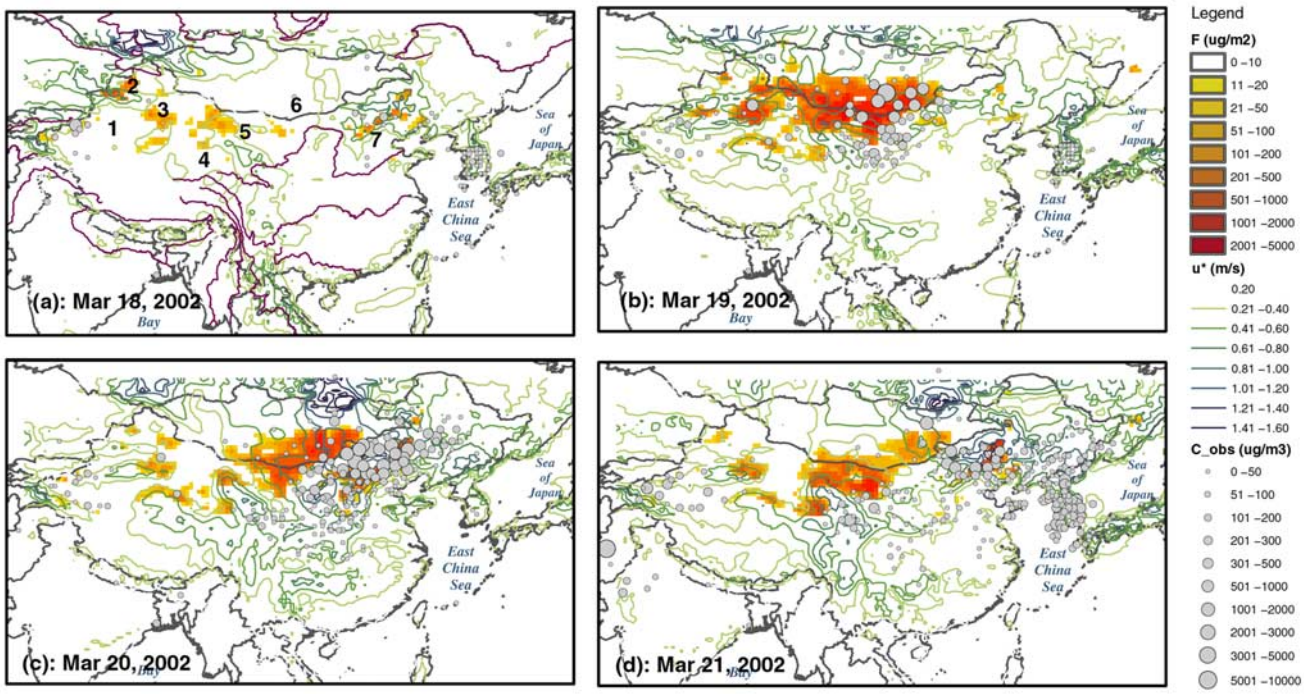

Figure 14. (a–d) Daily averaged dust emission in μg m^{-2} and friction velocity predicted by the integrated modeling system for the period of 18–21 March 2002. Near-surface dust concentrations derived from visibility are also shown for reference. In Figure 14a, the key regions of dust emission are enumerated. 1, Talimu Basin; 2, Zhunge'er Basin; 3, Tulufan Basin; 4, Chaidamu Basin; 5, Yellow River West Corridor; 6, Gobi Desert (central); 7, Gobi Desert (east).

receive net deposition. The magnitude of net deposition reaches up to 260 t km^{-2}. The Loess Plateau, situated immediately downstream of the Gobi Desert, is found to be the strongest dust sink, receiving about 100 t km^{-2} on average and 261 t km^{-2} at maximum. *Gao et al.* [1997] reported that (dry) dust depositions in Xi'an (109°E, 34°N), Lanzhou (104°E, 36°N) and Baotou (110°E, 41°N) are 19, 35 and 32 g m^{-2} mon^{-1}, respectively, corresponding to 38, 70 and 64 t km^{-2} in context of this study. Therefore the predicted dust deposition is consistent with the observations of *Gao et al.* [1997] Our finding is also consistent with the very geological fact that the Loess Plateau is formed largely

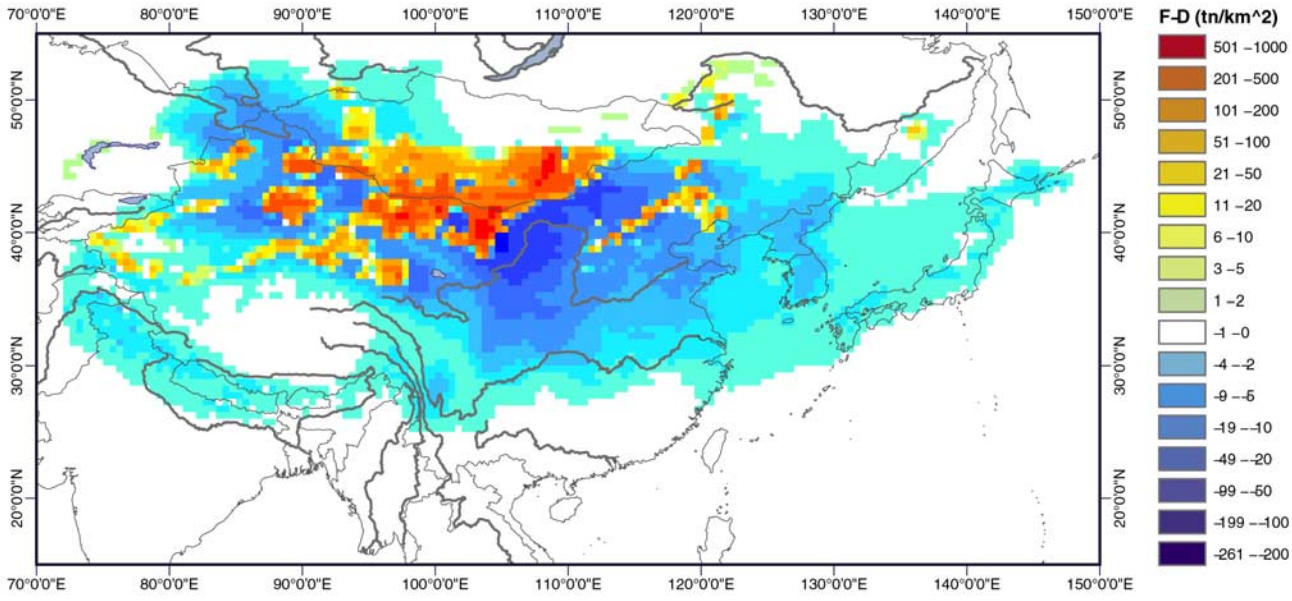

Figure 15. Predicted net cumulative dust flux in t km^{-2} for the period of March and April 2002.

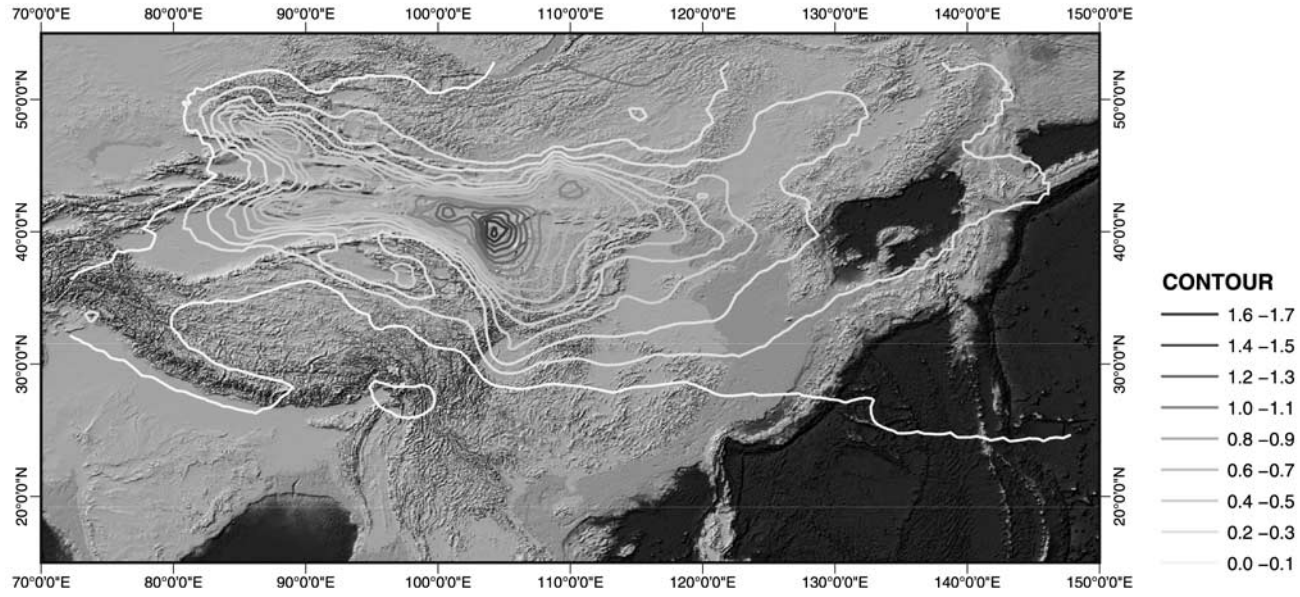

Figure 16. Average dust load in t km^{-2} as predicted by IWEAMS for the period of March and April 2002.

because of the deposition of wind transported particles over many millions of years.

[50] The existence of a deposition zone along the southern fringes of the Tibet Plateau is consistent with the frequent dust events observed there (refer to Figure 1, also *Shao and Wang* [2003]). An examination shows that dust in this area is originated from regions located to the southwest of the Tibet Plateau, including northwestern India, Pakistan, Afghanistan, etc.

[51] Figure 16 shows the average dust load. The quantity reaches up to 1.7 t km^{-2}. A high-dust-load zone is visible along the northern border of the Tibet Plateau. In the west, the high-dust-load zone is divided by the Tian Mountains into two horns, one stretching into the Talimu Basin and the other into the Zhunge'er Basin. In the east, the high-dust-load zone diverges downstream of the dust source region.

[52] Finally, we study the time series of total dust emission, total dust deposition and total dust load for the entire simulation domain. As shown in Figure 15, seven major dust episodes occurred in northeast Asia, as marked by the arrows. This is consistent with the (subjective) synoptic analysis summarized in Table 1, apart from that the dust episodes of 24–25 March, 30–31 March, 1–3 April, and 11 April cannot be clearly identified because they are localized events. The information presented in Figure 17 is further summarized in Table 4. The order of magnitude of dust emission is in broad agreement with that reported by *Ginoux et al.* [2003].

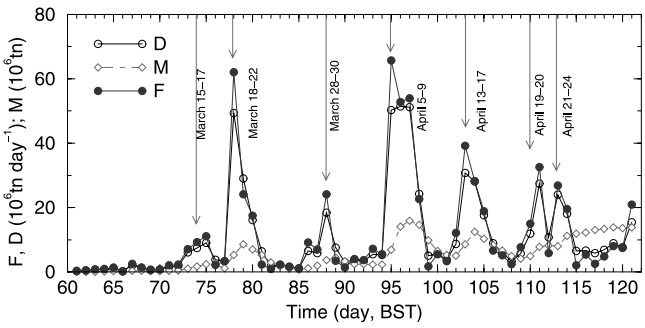

Figure 17. Variation of total dust emission, total dust deposition, and total dust load for the domain of simulation over the two-month period between March and April 2002. Major dust events are marked using arrows (see also Table 1).

6. Summary and Conclusions

[53] We have implemented IWEMS for the real-time forecast of northeast Asian dust storms for March and April 2002. The predicted quantities included dust emission, transport, deposition and concentration for various particle size groups. As the theory and the model framework have been previously published, [*Shao*, 2001; *Shao et al.*, 2002], the emphasis of this study has been placed on the validation of the predictions and on the quantification of the northeast Asian dust activities in terms of dust source, sink, concentration and load.

[54] The validation has been done as rigorously as the available observational data allow. Two data sets have been used for the purpose. The first data set consisted of the synoptic records and visibility observed at around 1200 weather stations, and the second data set consisted of the near-surface dust concentrations measured using low-volume samplers at 12 locations in China, Japan and Korea.

Table 4. Total Dust Emission, Total Dust Deposition, and Total Dust Load for the Simulation Domain

	Mean	Maximum
Total dust emission, $\times 10^6$ t d^{-1}	11.5	65.7
Total dust deposition, $\times 10^6$ t d^{-1}	10.8	51.4
Total dust load, $\times 10^6$ t	5.5	15.9

[55] The coincidence between the predicted and observed (derived from visibility using empirical relationships) near-surface dust concentration has been beyond the expectations of the authors: without any obvious exception, the spatial pattern and temporal evolution of the predicted and the observed dust concentration have shown very good agreement. This has been achieved without tuning any components or parameters of the modeling system. While the skill of the model decreases with forecast time, it has been found that even the 72-hour forecasts are still of high quality.

[56] We have predicted the concentrations of particle size groups of $d \leq 2$ μm, $d \leq 11$ μm and $d \leq 22$ μm, denoted as C_2, C_{11} and C_{TSP}, and compared these quantities with the measurements of Andersen samplers. Apart from the two stations in the Talimu Basin, good agreement has been found for C_{TSP} and C_{11}, but poor for C_2. This is not surprising, because the measured C_2 has a high percentage of particles from anthropogenic sources, while the predicted C_2 is purely for mineral particles from natural sources.

[57] We have attempted to compare the predictions with TOMS data (not shown), but found the latter is of too poor quality for the region and period concerned.

[58] On the basis of the predictions, we have examined the key terms for the quantification of dust activities in northeast Asia, including dust sources, sinks and dust load. Dust sources and intensity have been found to vary substantially in space and time during a dust episode, depending on the strength of winds and surface conditions. On average, the main source regions have been identified to be (1) the fringes of the Talimu Basin; (2) western Zhunge'er Basin; (3) the Tulufan Basin; (4) the Chaidamu Basin; (5) the Hexi Corridor; (6) Gobi Desert (central, including southern Mongolia and Inner Mongolia); and (7) Gobi Desert (east). The Gobi Desert (central) has been found to be the strongest source of dust emission, where the maximum dust emission rate is about 5000 μg m^{-2} s^{-1}.

[59] A proportion of dust emitted from the source regions is deposited back to the same regions, and thus it is important to examine net dust fluxes. We have examined the cumulative net dust flux for the simulation period and have found that net positive dust fluxes are mainly the deserts in inland China and southern Mongolia. These include the fringes of the Talimu Basin, the western part of the Zhunge'er Basin, the Tulufan Basin, the Chaidamu Basin and large areas of the Gobi Desert in southern Mongolia and Inner Mongolia as well as isolated locations along the southeastern fringes of the Gobi Desert. The Gobi Desert has the strongest net dust emission, reaching 1000 t km^{-2} over March and April 2002. Net negative dust flux (sink) covers a wide area: to the east and southeast, deposition areas include large parts of China, Bo Hai, the Yellow Sea, the East China Sea, the Korean Peninsula, Japan and Sea of Japan; to the west and northwest, deposition areas include parts of the Zhunge'er Basin (along the Altay Mountains) and parts of the Talimu Basin (along the Tian Mountains). Another net dust deposition area is the southern border of the Tibet Plateau. Dust particles deposited there are originated from dust sources further upstream, including northwestern India, Pakistan, Afghanistan, etc. We have found that the Loess Plateau, situated immediately downstream of the Gobi Desert, receives about 100 t km^{-2}, with a maximum of 261 t km^{-1}, over March and April 2002.

[60] The predictions have suggested that a zone of high dust load exists along the northern border of the Tibet Plateau, with a maximum of around 2 t km^{-2} over the Gobi. To the west, the high-dust-load zone is divided by the Tian Mountains into two horns, one stretching into the Talimu Basin and the other into the Zhunge'er Basin. To the east, the high-dust-load zone diverges downstream, spreading over large areas.

[61] We have determined the total dust emission, total dust deposition and total dust load for the entire domain of simulation and have found that the total dust emission is on average 11.5×10^6 t d^{-1} (maximum 65.7×10^6 t d^{-1}); total dust deposition is 10.8×10^6 t d^{-1} (maximum 51.4×10^6 t d^{-1}) and total dust load is 5.5×10^6 t with a maximum of 15.9×10^6 t.

[62] In recent years, several dust prediction models have been under development (e.g., *Wang et al.* [2000], *Nickovic et al.* [2001], *Song and Carmichael* [2001], *Uno et al.* [2001], *In and Park* [2002], *Barnum et al.* [2003], etc.). Much success has been reported, although the models have a varying degree of sophistication. On the basis of the present and the above-mentioned studies, it can be claimed with some confidence that the existing models have now the capacity for quantitative prediction of dust storms. With respect to the above-mentioned models, we have placed much emphasis on the soundness of the dust emission scheme, the reliability of land surface parameters and the integration of dynamic models with spatial data. This effort has significantly improved the reliability and accuracy of model forecasts as illustrated by the comparisons presented in this study.

[63] **Acknowledgments.** The results presented in this study arise from a collaborative project to which many colleagues contributed. The senior author wishes to express his thanks for the support and encouragement of Q. C. Zeng, G. B. Peng, H. Li, and G. C. Zhang. Colleagues Z. Y. Fang, S. X. Zhao, N. M. Lu, Z. D. Yang, L. Ma, S. Y. Cai, W. Wang, J. H. Sun, and L. N. Zhao have participated in the discussions. The effort of M. Mikami in facilitating the collaboration between the Chinese and Japanese scientists is gratefully acknowledged. The project is supported by the Ministry of Finance of China (Y0101) and the Hong Kong Research Grants Council (project 9040748).

References

Alfaro, S. C., and L. Gomes, Modelling mineral aerosol production by wind erosion: Emission intensities and aerosol size distributions in source areas, *J. Geophys. Res.*, *106*, 18,075–18,084, 2001.

Barnum, B. H., N. S. Winstead, J. Wesely, L. A. Hakola, P. R. Colarco, O. B. Toon, P. Ginoux, G. Brooks, L. Hasselbarth, and B. Toth, Forecasting dust storms using the CARMA-dust model and MM5 weather data, *Environ. Modell. Software*, in press, 2003.

Chatenet, B., B. Marticorena, L. Gomes, and G. Bergametti, Assessing the microped size distributions of desert soils erodible by wind, *Sedimentology*, *43*, 901–911, 1996.

Dong, Z. B., X. M. Wang, and L. Y. Liu, Wind erosion in arid and semiarid China: An overview, *J. Soil Water Conserv.*, *55*, 439–444, 2000.

Gao, Y., R. Arimoto, R. A. Duce, X. Y. Zhang, G. Y. Zhang, Z. S. An, L. Q. Chen, M. Y. Zhou, and D. Y. Gu, Temporal and spatial distributions of dust and its deposition to the China Sea, *Tellus, Ser. B*, *49*, 172–189, 1997.

Gillette, D. A., and K. J. Hanson, Spatial and temporal variability of dust production caused by wind erosion in the United States, *J. Geophys. Res.*, *94*, 2197–2206, 1989.

Ginoux, P., J. Prospero, O. Torres, and M. Chin, Long-term simulation of global dust distribution with the GOCART model: Correlation with the North Atlantic Oscillation, *Environ. Modell. Software*, in press, 2003.

Gomes, L., G. Bergametti, G. Coude-Gaussen, and P. Rognon, Submicron desert dusts: A sandblasting process, *J. Geophys. Res.*, *95*, 13,927–13,935, 1990.

Husar, R. B., et al., Asian dust events of April 1998, *J. Geophys. Res.*, *106*, 18,317–18,330, 2001.

In, H. J., and S. U. Park, A simulation of long-range transport of Yellow Sand observed in April 1998 in Korea, *Atmos. Environ.*, *36*, 4173–4187, 2002.

Irannejad, P., and Y. Shao, Description and validation of the Atmosphere-Land-Surface Interaction Scheme (ALSIS) with HAPEX and Cabauw data, *Global. Planet. Change*, *19*, 87–114, 1998.

Joussaume, S., Three-dimensional simulation of the atmospheric cycle of desert dust particles using a general circulation model, *J. Geophys. Res.*, *95*, 1909–1941, 1990.

Kanai, Y., et al., Preliminary study on the grain-size distribution and concentration of aeolian dust collected in Japan, *J. Arid Land Stud.*, *11*, 307–314, 2002.

Lu, H., and Y. Shao, A new model for dust emission by saltation bombardment, *J. Geophys. Res.*, *104*, 16,827–16,842, 1999.

Lu, H., and Y. Shao, Toward quantitative prediction of dust storms: An integrated wind erosion modelling system and its applications, *Environ. Modell. Software*, *16*, 233–249, 2001.

Marticorena, B., and G. Bergametti, Modeling the atmospheric dust cycle: 1. Design of a soil-derived dust emission scheme, *J. Geophys. Res.*, *100*, 16,415–16,430, 1995.

Marticorena, B., G. Bergametti, B. Aumont, Y. Callot, C. N'Doume, and M. Legrand, Modeling the atmospheric dust cycle: 2. Simulation of Saharan dust sources, *J. Geophys. Res.*, *102*, 4387–4404, 1997.

Mikami, M., et al., The impact of aeolian dust on climate: Sino-Japanese cooperative project ADEC, *J. Arid Land Stud.*, *11*, 211–222, 2002.

Nickovic, S., S. Kallos, A. Papadopoulos, and O. Kakaliagou, A model for prediction of desert dust cycle in the atmosphere, *J. Geophys. Res.*, *106*, 18,113–18,129, 2001.

Owen, R. P., Saltation of uniform grains in air, *J. Fluid Mech.*, *20*, 225–242, 1964.

Prospero, J. M., P. Ginoux, O. Torres, S. E. Nicholson, and T. E. Gill, Environmental characterization of global sources of atmospheric soil dust identified with the Nimbus 7 Total Ozone Mapping Spectrometer (TOMS) absorbing aerosol product, *Rev. Geophys.*, *40*, 2–31, 2002.

Raupach, M. R., P. R. Briggs, N. Ahmad, and V. E. Edge, Endosulfan transport II: Modelling airborne dispersal and deposition by spray and vapour, *J. Environ. Qual.*, *30*, 729–740, 2001.

Shao, Y., A model for mineral dust emission, *J. Geophys. Res.*, *106*, 20,239–20,254, 2001.

Shao, Y., and L. M. Leslie, Wind erosion prediction over the Australian continent, *J. Geophys. Res.*, *102*, 30,091–30,105, 1997.

Shao, Y., and H. Lu, A simple expression for wind erosion threshold friction velocity, *J. Geophys. Res.*, *105*, 22,437–22,443, 2000.

Shao, Y., and L. Wang, A climatology of northeast Asian dust events, *Meteorol. Z.*, *12*, 187–196, 2003.

Shao, Y., M. R. Raupach, and J. F. Leys, A model for predicting aeolian sand drift and dust entrainment on scales from paddock to region, *Aust. J. Soil Res.*, *34*, 309–342, 1996.

Shao, Y., E. J. Jung, and L. M. Leslie, Numerical prediction of northeast Asian dust storms using an integrated wind erosion modeling system, *J. Geophys. Res.*, *107*, 4814–4836, 2002.

Sokolik, I. N., O. B. Toon, and R. W. Bergstrom, Modeling of radiative characteristics of airborne mineral aerosols at infrared wavelengths, *J. Geophys. Res.*, *103*, 8813–8826, 1998.

Song, C. H., and G. R. Carmichael, A three-dimensional modeling investigation of the evolution processes of dust and sea-salt particles in east Asia, *J. Geophys. Res.*, *106*, 18,131–18,154, 2001.

Uno, I., H. Amano, S. Emori, K. Kinoshita, I. Matsui, and N. Sugimoto, Trans-Pacific yellow sand transport observed in April 1998: A numerical simulation, *J. Geophys. Res.*, *106*, 18,331–18,344, 2001.

Wang, Z., H. Ueda, and M. Huang, A deflation module for use in modeling long-range transport of yellow sand over east Asia, *J. Geophys. Res.*, *105*, 26,947–26,957, 2000.

Westphal, D. L., O. B. Toon, and T. N. Carson, A case study of mobilisation and transport of Saharan dust, *J. Atmos. Sci.*, *45*, 2145–2175, 1988.

Yabuki, S., S. Kanayama, F. F. Fu, M. Honda, F. Yanagisawa, W. S. Wei, F. J. Zeng, M. H. Liu, Z. B. Shen, and L. C. Liu, Physical and chemical characteristics of aeolian dust collected over Asian dust source regions in China: Comparison with atmospheric aerosols in an urban area at Wako, Japan, *J. Arid Land Stud.*, *11*, 273–289, 2002.

Zhang, G. P., Z. X. Zhang, and J. Y. Liu, Spatial distribution of aeolian erosion of soil and its driving factors in China (in Chinese), *Acta Geogr. Sin.*, *56*, 146–158, 2001.

Zhou, Z. J., Blowing sand and sand storm in China in recent 45 years (in Chinese), *Quat. Sci.*, *21*, 9–17, 2001.

Y. Chun, Applied Meteorology Research Laboratory, Meteorological Research Institute/KMA 460-18, Shindaebang-dong, Dongjak-ku, Seoul 156-720, Korea. (yschun@metri.re.kr)

C. Dong, National Satellite Meteorology Centre, China Meteorological Administration, 46 Zhongguancun South Street, Beijing, China 100081. (dchua@nsmc.cma.gov.cn)

Y. Kanai, National Institute of Advanced Industrial Science and Technology, Geological Survey of Japan, 1-1-1 Higashi, Tsukuba, Ibaraki 305-8567, Japan. (y.kanai@aist.go.jp)

L. M. Leslie, School of Meteorology, University of Oklahoma, 100 East Boyd Street, Room 1310, Norman, OK 73019, USA. (lmleslie@ou.edu)

Z. Lin, Institute of Atmospheric Physics, Chinese Academy of Sciences, Beijing, China 100029. (lzh@mail.iap.ac.cn)

Y. Shao and Y. Yang, Department of Physics and Materials Science, City University of Hong Kong, Hong Kong, China. (apyshao@cityu.edu.hk)

Z. Song and J. Wang, National Meteorology Centre, China Meteorological Administration, 46 Zhongguancun South Street, Beijing, China 100081. (wangjj@cma.gov.cn; songzx@cma.gov.cn)

S. Yabuki, Institute of Physical and Chemical Research, 2-1 Hirosawa, Wako, Saitama 351-0198, Japan. (syabuki@riken.go.jp)

Z. Zhang, Institute of Geographical Sciences and Natural Resources Research, Chinese Academy of Sciences, Beijing, China 100101. (zhangsh@www.lreis.ac.cn)